Advances in Applied Mathematics and Mechanics
Adv. Appl. Math. Mech., Vol. **xx**, No. x, pp. 1-23

DOI: 10.4208/aamm.OA-2020-0138
xx 202x

High-Order Well-Balanced Finite Volume WENO Schemes with Conservative Variables Decomposition for Shallow Water Equations

Jiaojiao Li, Gang Li*, Shouguo Qian* and Jinmei Gao

School of Mathematics and Statistics, Qingdao University, Qingdao, Shandong 266071, China

Received 17 May 2020; Accepted (in revised version) 20 September 2020

Abstract. This article presents well-balanced finite volume weighted essentially non-oscillatory (WENO) schemes to solve the shallow water equations (SWEs). Well-balanced schemes are characterized by preservation of the steady state exactly at the discrete level. The well-balanced property is of paramount importance in practical applications where many studied phenomena are regarded as small perturbations to equilibrium states. To achieve the well-balanced property, numerical fluxes presented here are constructed by means of a suitable conservative variables decomposition and the hydrostatic reconstruction idea. This decomposition strategy allows us to realize a novel simple source term approximation. Both rigorous theoretical analysis and extensive numerical examples all verify that the resulting schemes maintain the well-balanced property exactly. Furthermore, numerical results strongly imply that the proposed schemes can accurately capture small perturbations to the steady state and keep the genuine high-order accuracy for smooth solutions.

AMS subject classifications: 74S05

Key words: Shallow water equations, source term, WENO schemes, well-balanced property, hydrostatic reconstruction, conservative variables decomposition.

1 Introduction

The SWEs play a main role in the fields of hydraulic science and coastal engineering [1–3]. This article is concerned with developing high-order schemes for the SWEs over a non-

*Corresponding author.
Emails: jiaojiaojiao807@163.com (J. J. Li), gangli1978@163.com (G. Li), sgqian1976@163.com (S. G. Qian), gjinmei1979@163.com (J. M. Gao)

flat bottom topography, which in the one space dimension enjoy the following form

$$h_t+(hu)_x=0, \tag{1.1a}$$

$$(hu)_t+\left(hu^2+\frac{1}{2}gh^2\right)_x=-ghb_x, \tag{1.1b}$$

where $h(x,t)$, $u(x,t)$, $b(x)$ stand for the water depth, the depth-averaged flow velocity, and the bottom topography, respectively. The notations x and t are the space and time, while the real constant $g=9.812\mathrm{m/s}^2$ denotes the gravitational constant. The original system (1.1) can be rewritten into the following vector form

$$U_t+F(U)_x=S(U,b), \tag{1.2}$$

with $U=(h,hu)^T$, $F(U)=\left(hu,hu^2+\frac{1}{2}gh^2\right)^T$ and $S(U,b)=(0,-ghb_x)^T$ being the unknown conservative variables, the physical flux and the geometrical source term, respectively.

The system (1.1) belongs to the hyperbolic conservation laws (also referred as hyperbolic balance laws). Hyperbolic balance laws generally possess the form like (1.2), and have received growing consideration in the past decades. The balance laws usually allow the existence of non-trivial steady state solutions, in which the flux gradient is non-zero and is balanced by the geometricial source term exactly. Concerning the 1D SWEs, the well-known equilibrium state is the so-called still water steady state solutions

$$u=0, \quad h+b=\text{constant}. \tag{1.3}$$

The SWEs are highly nonlinear, such that analytical treatment on them is extremely difficult. Therefore, numerical computation has become a key means in studying SWEs. Furthermore, the above steady states and their small perturbations are of great interest in practical applications, and can not be commonly captured by standard schemes with direct treatment of the source term. In particular, this will lead to spurious oscillations even with very refined mesh. Moreover, the mesh refinement strategy will not eliminate the oscillations and only reduce the magnitude of the oscillations. Furthermore, such strategy is impractical due to high computational cost, especially for multi-dimensional problems.

To save the computational cost, well-balanced schemes [4, 5] have been proposed to exactly maintain the still water steady state up to machine accuracy at the discrete level. In comparison with the non-well-balanced counterpart, the well-balanced schemes can also resolve small perturbations of the steady state even on relatively coarse mesh [6, 7], and save the computational cost considerably, then improve the efficiency greatly. Following the pioneering works [4, 5], many researchers have attempted on this subject. Many representative research results include: kinetic scheme [8], gas-kinetic scheme [9], central-upwind scheme [10], finite volume evolution Galerkin method [11], WENO schemes [12–18], Hermite WENO scheme [19], central schemes [20, 21], discontinuous Galerkin (DG) methods [16, 22], ADER schemes [23, 24], spectral element method [25],

weighted compact schemes [26], element-free Galerkin method [27], and so on. About the latest progresses of this subject, we refer to the book by Gosse [28], while for a brief historic review, we refer to [6,29].

It is noteworthy that Audusse et al. [30,31] originally introduce the hydrostatic reconstruction idea to build well-balanced finite volume schemes. Afterwards, finite volume WENO scheme and DG method [32,33] have been developed following the original idea in [30,31].

The key objective of this article is to develop high-order well-balanced finite volume WENO scheme for SWEs at the still water steady state. The resulting scheme enjoys the following novel features:

- A proper decomposition strategy is introduced for the conservative variables, which are decomposed into equilibrium part and residual part.
- Well-balanced numerical flux is constructed by means of the decomposition strategy and the hydrostatic reconstruction idea.
- The decomposition strategy allows us to realize a simple source term approximation, which is compatible with the approximation to the flux gradient.

The proposed scheme possesses the following properties:

- It is well-balanced for one- and two-dimensional SWEs with still water steady state solutions.
- It keeps high-order accuracy for smooth solutions with the aid of the high-order WENO reconstruction.

In summary, the decomposition strategy simplifies the realization of the well-balanced property.

This article is organized as follows: Section 2 focuses on the construction of well-balanced finite volume WENO schemes for one- and two-dimensional SWEs. Section 3 devotes to present numerical experiments and conclusions are drawn in Section 4.

2 Construction of finite volume WENO schemes for the SWEs

We first subdivide the domain $[a,b]$ into N cells with $I_j=[x_{j-\frac{1}{2}},x_{j+\frac{1}{2}}]$ for $j=1,\cdots,N$, where $a=x_{\frac{1}{2}}<x_{\frac{3}{2}}<\cdots<x_{N+\frac{1}{2}}=b$. In addition, we denote the cell center and the uniform mesh size by $x_j=\frac{1}{2}(x_{j-\frac{1}{2}}+x_{j+\frac{1}{2}})$ and $\Delta x=\frac{b-a}{N}$, respectively. In the framework of finite volume schemes, we look for $\overline{U}_j(t)$ to approximate the cell average

$$\overline{U}(x_j,t)=\frac{1}{\Delta x}\int_{I_j}U(x,t)dx.$$

The semi-discrete conservative finite volume schemes are defined in the following form.

To achieve the well-balanced property, we propose a decomposition strategy for the unknown variables and follow the hydrostatic reconstruction idea in the building of the numerical flux. In this article, our semi-discrete finite volume WENO schemes for the one-dimensional shallow water equations (1.2) enjoy the following form:

$$\frac{d}{dt}\overline{U}_j(t)+\frac{1}{\Delta x}\left(\widehat{F}^l_{j+\frac{1}{2}}-\widehat{F}^r_{j-\frac{1}{2}}\right)=\frac{1}{\Delta x}\int_{I_j}S(U,b)dx. \tag{2.1}$$

Here $\widehat{F}^l_{j+\frac{1}{2}}$ and $\widehat{F}^r_{j-\frac{1}{2}}$ denote numerical fluxes and are used to approximate the physical fluxes at cell interfaces from the left side and the right side, i.e., $F(U(x^-_{j+\frac{1}{2}}))$ as well as $F(U(x^+_{j-\frac{1}{2}}))$, respectively.

2.1 Modified WENO reconstruction at cell interfaces

Concerning the still water steady state (1.3), it is evident that $\bar{h}_j+\bar{b}_j=$constant. To achieve the well-balanced WENO schemes, the reconstructed values at the cell interfaces should satisfy the following goals

$$h^+_{j-\frac{1}{2}}+b^+_{j-\frac{1}{2}}=\text{constant}\quad\text{and}\quad h^-_{j+\frac{1}{2}}+b^-_{j+\frac{1}{2}}=\text{constant},$$

where $h^\pm$ and $b^\pm$ are obtained by the WENO reconstruction. Herein, we adopt a similar approach as in [32] to achieve the above goal. Firstly, with the cell averages $\overline{U}=(\bar{h},\overline{hu})^T$ at hands, and by the WENO reconstruction, we obtain the reconstructed values

$$U^+_{j-\frac{1}{2}}=\sum_{k=-r+1}^{r-1}c_k\overline{U}_{j+k},\quad U^-_{j+\frac{1}{2}}=\sum_{k=-r+1}^{r-1}\tilde{c}_k\overline{U}_{j+k}. \tag{2.2}$$

The coefficients c_k and $\tilde{c}_k$ depend nonlinearly on the smoothness indicators involving $\{\overline{U}_j\}$ and satisfy

$$\sum_{k=-r+1}^{r-1}c_k=1,\quad\sum_{k=-r+1}^{r-1}\tilde{c}_k=1,$$

due to the compatibility of the WENO reconstruction. Then, we adopt the reconstruction procedure with the same coefficients c_k and $\tilde{c}_k$ in (2.2) on $\overline{B}=(\bar{b},0)^T$ and get

$$B^+_{j-\frac{1}{2}}=\sum_{k=-r+1}^{r-1}c_k\overline{B}_{j+k}\quad\text{and}\quad B^-_{j+\frac{1}{2}}=\sum_{k=-r+1}^{r-1}\tilde{c}_k\overline{B}_{j+k}. \tag{2.3}$$

Therefore, Eqs. (2.2) and (2.3) lead to

$$U^+_{j-\frac{1}{2}}+B^+_{j-\frac{1}{2}}=\sum_{k=-r+1}^{r-1}c_k\left(\overline{U}_{j+k}+\overline{B}_{j+k}\right), \tag{2.4a}$$

$$U^-_{j+\frac{1}{2}}+B^-_{j+\frac{1}{2}}=\sum_{k=-r+1}^{r-1}\tilde{c}_k\left(\overline{U}_{j+k}+\overline{B}_{j+k}\right), \tag{2.4b}$$

and ultimately bring about the following results

$$h^+_{j-\frac{1}{2}}+b^+_{j-\frac{1}{2}}=\text{constant}\quad\text{and}\quad h^-_{j+\frac{1}{2}}+b^-_{j+\frac{1}{2}}=\text{constant} \tag{2.5}$$

on account of the consistence of the WENO reconstruction as well as the equality $\bar{h}_j+\bar{b}_j=$ constant. For more information about the WENO reconstruction, we refer to the note [34] and the reviews [35,36] for the more recent progress.

Then, we apply the following three steps:

1. we first decompose the reconstructed values at the cell interface into two parts, i.e., equilibrium part and residual part, through a decomposition strategy.
2. Secondly, we construct the well-balanced numerical fluxes based on the decomposition strategy and the hydrostatic reconstruction idea [30,31].
3. Thirdly, we propose a novel source term approximation in view of the decomposition to the Gaussian quadrature grid values.

Remark 2.1. With regard to systems of hyperbolic balance laws, the WENO reconstruction is always adopted in combination with a local characteristic decomposition, see e.g., [34,35]. Thanking to the local characteristic decomposition, the computational cost will increase, however the resulting scheme is more robust and leads to better numerical results with less oscillations, if compared to schemes only with a simple WENO reconstruction in a component by component fashion. For two-dimensional problems, the reconstruction procedure is based on a dimension by dimension splitting.

2.2 Decomposition technique for conservative variables at cell interfaces

By means of the WENO reconstruction, we get

$$U^+_{j-\frac{1}{2}}=\left(h^+_{j-\frac{1}{2}},(hu)^+_{j-\frac{1}{2}}\right)^T\quad\text{and}\quad U^-_{j+\frac{1}{2}}=\left(h^-_{j+\frac{1}{2}},(hu)^-_{j+\frac{1}{2}}\right)^T$$

at hands. Then, we decompose the reconstructed values at cell interfaces into an equilibrium part U^e and a residual part U^r as described below. On one hand, a natural choice for the flow velocity at the equilibrium state is as follows:

$$u^{e,+}_{j-\frac{1}{2}}=0\quad\text{and}\quad u^{e,-}_{j+\frac{1}{2}}=0.$$

On the other hand, we take

$$h^{e,+}_{j-\frac{1}{2}}=\bar{h}_j+\bar{b}_j-b^+_{j-\frac{1}{2}} \quad \text{and} \quad h^{e,-}_{j+\frac{1}{2}}=\bar{h}_j+\bar{b}_j-b^-_{j+\frac{1}{2}}$$

as the equilibrium part of the water depth. Then, we decompose the reconstructed values at cell interfaces as follows:

$$U^+_{j-\frac{1}{2}}=U^{e,+}_{j-\frac{1}{2}}+U^{r,+}_{j-\frac{1}{2}} \quad \text{and} \quad U^-_{j+\frac{1}{2}}=U^{e,-}_{j+\frac{1}{2}}+U^{r,-}_{j+\frac{1}{2}} \tag{2.6}$$

with

$$U^{e,+}_{j-\frac{1}{2}}=\left(h^{e,+}_{j-\frac{1}{2}},(hu)^{e,+}_{j-\frac{1}{2}}\right)^T=\left(h^{e,+}_{j-\frac{1}{2}},0\right)^T, \tag{2.7a}$$

$$U^{e,-}_{j+\frac{1}{2}}=\left(h^{e,-}_{j+\frac{1}{2}},(hu)^{e,-}_{j+\frac{1}{2}}\right)^T=\left(h^{e,-}_{j+\frac{1}{2}},0\right)^T, \tag{2.7b}$$

and

$$U^{r,+}_{j-\frac{1}{2}}=U^+_{j-\frac{1}{2}}-U^{e,+}_{j-\frac{1}{2}} \quad \text{and} \quad U^{r,-}_{j+\frac{1}{2}}=U^-_{j+\frac{1}{2}}-U^{e,-}_{j+\frac{1}{2}} \tag{2.8}$$

being the equilibrium part and the residual part, respectively. Moreover, at the still water steady state, we have the following fact that $U^{r,+}_{j-\frac{1}{2}}=U^{r,-}_{j+\frac{1}{2}}=0$ due to Eq. (2.5) in Section 2.1 and Eqs. (2.6)–(2.8).

2.3 Construction of numerical flux based on hydrostatic reconstruction

Failure to achieve the well-balanced property is mainly due to two aspects: the approximation to the flux gradient cannot be offset by the one to the source term; the numerical flux is not consistent with the physical flux at the cell interface. Therefore, the construction of numerical fluxes $\widehat{F}^r_{j-\frac{1}{2}}$ and $\widehat{F}^l_{j+\frac{1}{2}}$ in (2.1) is crucial to the preservation of the well-balanced property. In this article, the numerical fluxes are required to satisfy the following conditions

$$\widehat{F}^r_{j-\frac{1}{2}}=F\left(U^+_{j-\frac{1}{2}}\right) \quad \text{and} \quad \widehat{F}^l_{j+\frac{1}{2}}=F\left(U^-_{j+\frac{1}{2}}\right) \tag{2.9}$$

at the still water steady state (1.3) and possess the following forms

$$\widehat{F}^r_{j-\frac{1}{2}}=\hat{f}\left(U^{*,-}_{j-\frac{1}{2}},U^{*,+}_{j-\frac{1}{2}}\right)+F\left(U^+_{j-\frac{1}{2}}\right)-F\left(U^{*,+}_{j-\frac{1}{2}}\right), \tag{2.10a}$$

$$\widehat{F}^l_{j+\frac{1}{2}}=\hat{f}\left(U^{*,-}_{j+\frac{1}{2}},U^{*,+}_{j+\frac{1}{2}}\right)+F\left(U^-_{j+\frac{1}{2}}\right)-F\left(U^{*,-}_{j+\frac{1}{2}}\right). \tag{2.10b}$$

Here,

$$\hat{f}(a_1,a_2)=\frac{1}{2}\left(F(a_1)+F(a_2)-\alpha(a_2-a_1)\right) \tag{2.11}$$

denotes the simple and efficient Lax-Friedrichs flux with $\alpha=\max\left|u+\sqrt{gh}\right|$ over the whole computational domain.

We will adopt the following procedures to realize the aim (2.9).

In addition, the notation U^* stands for the value obtained with the hydrostatic reconstruction. Specifically speaking, inspired by the the hydrostatic reconstruction idea [30], we locally redefine the cell interface values as follows

$$U^{*,+}_{j-\frac{1}{2}}=\left(\bar{h}_j+\bar{b}_j-b^*_{j-\frac{1}{2}},0\right)^T+U^{r,+}_{j-\frac{1}{2}}, \tag{2.12a}$$

$$U^{*,-}_{j+\frac{1}{2}}=\left(\bar{h}_j+\bar{b}_j-b^*_{j+\frac{1}{2}},0\right)^T+U^{r,-}_{j+\frac{1}{2}}, \tag{2.12b}$$

with

$$b^*_{j\pm\frac{1}{2}}=\max\left(b^-_{j\pm\frac{1}{2}},b^+_{j\pm\frac{1}{2}}\right).$$

2.4 Source term approximation with decomposition technique

To realize the well-balanced schemes, the approximation to source term is required to balance the one to the flux gradient. In view of the linearity of the source term $S(U,b)$ with respect to U, (i.e., $S(U,b)=S(U^e,b)+S(U^r,b)$), the cell intergration $\int_{I_j}S(U,b)dx$ in (2.1) can be decomposed into as follows

$$\int_{I_j}S(U,b)dx=\int_{I_j}S(U^e,b)dx+\int_{I_j}S(U^r,b)dx. \tag{2.13}$$

At the still water steady state, the balancing $F(U^e)_x=S(U^e,b)$ with U^e as the eqilibrium state leads to the following equality

$$\int_{I_j}S(U^e,b)dx=\int_{I_j}F(U^e)_xdx=F\left(U^{e,-}_{j+\frac{1}{2}}\right)-F\left(U^{e,+}_{j-\frac{1}{2}}\right). \tag{2.14}$$

For another cell integration

$$\int_{I_j}S^{(2)}(U^r,b)dx=\int_{I_j}-gh^rb_xdx$$

in the second equation, we apply the three-point Gaussian quadrature rule. Concretely speaking, we first get h_{G_k}, b_{G_k}, $k=1,2,3$, as the Gaussian point values of h and b by the WENO reconstruction. Next, we define the Gaussian point values of h under the steady state as follows:

$$h^e_{G_k}=\bar{h}_j+\bar{b}_j-b_{G_k},\quad k=1,2,3,$$

then get

$$h^r_{G_k}=h_{G_k}-h^e_{G_k},\quad k=1,2,3.$$

To realize $h_{G_k}+b_{G_k}=$constant, we implement the WENO reconstruction to $\overline{U}=(\bar{h},\overline{hu})^T$ firstly and obtain h_{G_k}, $k=1,2,3$ secondly. Afterwards, we adopt the same coefficients for $\overline{U}$ to the WENO reconstruction for $\overline{B}=(\bar{b},0)^T$, then get b_{G_k}, $k=1,2,3$ correspondingly. In fact, the procedures to realize $h_{G_k}+b_{G_k}=$constant, $k=1,2,3$, are similar to those in (2.2), (2.3) and (2.4).

2.5 The temporal discretization

Now, the semi-discrete schemes (2.1) can be written out as an ordinary differential equation:

$$\frac{d}{dt}\overline{U}(t)=\mathcal{F}(\overline{U}) \tag{2.15}$$

with $\mathcal{F}(\overline{U})$ being a spatial operator including the approximations to both the flux gradient and the source term in (2.1). For the temporal discretization, we apply the third-order Runge-Kutta approach [37]:

$$\overline{U}^{(1)}=\overline{U}^n+\Delta t\mathcal{F}\left(\overline{U}^n\right), \tag{2.16a}$$

$$\overline{U}^{(2)}=\frac{3}{4}\overline{U}^n+\frac{1}{4}\left(\overline{U}^{(1)}+\Delta t\mathcal{F}\left(\overline{U}^{(1)}\right)\right), \tag{2.16b}$$

$$\overline{U}^{n+1}=\frac{1}{3}\overline{U}^n+\frac{2}{3}\left(\overline{U}^{(2)}+\Delta t\mathcal{F}\left(\overline{U}^{(2)}\right)\right). \tag{2.16c}$$

2.6 Implementation details of the finite volume WENO schemes

The complete algorithm of the current schemes can be summarized as follows:

1. Starting from the initial data, we get the cell averages $\{\overline{U}_j\}$ and $\{\bar{b}_j\}$,

2. By means of the WENO reconstruction with modification in Section 2, we obtain $U^{\pm}_{j\pm\frac{1}{2}}$ as well as $b^{\pm}_{j\pm\frac{1}{2}}$ at the cell interfaces. Then, we decompose $U^{\pm}$ with the following form
$$U^{+}_{j-\frac{1}{2}}=U^{e,+}_{j-\frac{1}{2}}+U^{r,+}_{j-\frac{1}{2}} \quad \text{and} \quad U^{-}_{j+\frac{1}{2}}=U^{e,-}_{j+\frac{1}{2}}+U^{r,-}_{j+\frac{1}{2}},$$

3. Construct numerical fluxes $\widehat{F}^r_{j-\frac{1}{2}}$ and $\widehat{F}^l_{j+\frac{1}{2}}$ as in (2.10) with the the hydrostatic reconstruction idea through (2.12),

4. Approximate the source term as in (2.13),

5. Update the numerical solutions to the next time level and get $\overline{U}^{n+1}$ by the aid of the Runge-Kutta approach (2.16).

2.7 Analysis of the well-balanced schemes

All the above treatments together result in well-balanced schemes, which maintain the steady state at the discrete level.

Theorem 2.1. *With respect to the one-dimensional SWEs* (1.1)*, the proposed finite volume WENO schemes* (2.1)*, combined with the numerical fluxes* (2.10) *and the source term approximation* (2.13)*, are well-balanced for the still water steady state* (1.3)*.*

Proof. For the still water steady state (1.3), any consistent scheme is exact for the first equation $(hu)_x=0$ since $u=0$. Concerning the well-balanced property, we only focus on the second equation.

In terms of $U^{e,+}_{j-\frac{1}{2}}$ and $U^{e,-}_{j+\frac{1}{2}}$ in (2.7), we observe the following facts

$$U^{e,+}_{j-\frac{1}{2}}=U^{+}_{j-\frac{1}{2}} \quad \text{and} \quad U^{e,-}_{j+\frac{1}{2}}=U^{-}_{j+\frac{1}{2}},$$

due to $U^{r,+}_{j-\frac{1}{2}}=U^{r,-}_{j+\frac{1}{2}}=0$ at the still water steady state. In addition, we also have $h^r_{G_k}=0$, $k=1,2,3$, which lead to

$$\int_{I_j}-gh^r b_x dx=0.$$

Then, the source term approximation reduces to

$$\int_{I_j}S(U,b)dx=F\left(U^{e,-}_{j+\frac{1}{2}}\right)-F\left(U^{e,+}_{j-\frac{1}{2}}\right)=F\left(U^{-}_{j+\frac{1}{2}}\right)-F\left(U^{+}_{j-\frac{1}{2}}\right)$$

in combination with (2.13) and (2.14).

Moreover, in the case of lake at rest steady state, we own the following equality

$$U^{*,-}_{j\pm\frac{1}{2}}=U^{*,+}_{j\pm\frac{1}{2}}$$

due to $\overline{(h+b)}_j\equiv$constant and $U^{r,+}_{j-\frac{1}{2}}=U^{r,-}_{j+\frac{1}{2}}=0$. Subsequently, we have

$$\widehat{F}^r_{j-\frac{1}{2}}=F\left(U^{+}_{j-\frac{1}{2}}\right) \quad \text{and} \quad \widehat{F}^l_{j+\frac{1}{2}}=F\left(U^{-}_{j+\frac{1}{2}}\right)$$

thanks to the consistence of the Lax–Friedrichs flux in (2.11), i.e., $\hat{f}(a,a)=F(a)$.

Finally, we conclude that the source term approximation in (2.14) is exactly balanced by the one to the flux gradient, namely,

$$\int_{I_j}S(U,b)dx=\widehat{F}^l_{j+\frac{1}{2}}-\widehat{F}^r_{j-\frac{1}{2}},$$

which indicates the desired well-balanced property at the discrete level. This finishes the proof. □

2.8 The two-dimensional cases

The two-dimensional SWEs take the following form

$$h_t+(hu)_x+(hv)_y=0, \tag{2.17a}$$

$$(hu)_t+\left(hu^2+\frac{1}{2}gh^2\right)_x+(huv)_y=-ghb_x, \tag{2.17b}$$

$$(hv)_t+(huv)_x+\left(hv^2+\frac{1}{2}gh^2\right)_y=-ghb_y, \tag{2.17c}$$

where $v(x,y,t)$ denotes the flow velocity in the y direction. The other notations are the same as in the one-dimensional cases. Here, the still water steady state we are interested to maintain is as follows

$$u=v=0, \quad h+b=\text{constant}.$$

It is straightforward to generalize the proposed one-dimensional well-balanced schemes to the above two-dimensional SWEs (2.17).

3 Numerical results

Herein, we implement extensive examples to validate the performances of the current schemes. Throughout the article, we apply the fifth-order (i.e., $r=3$) WENO reconstruction for the spatial discretization and employ the third-order Runge-Kutta approach (2.16) for the temporal discretization. The CFL number is taken as 0.6 to maintain the numerical stability, except for the accuracy testing where we take smaller time step to ensure that spatial errors dominate.

3.1 One-dimensional cases

3.1.1 Testing the well-balanced property

To testify the well-balanced property, we use an example in [14] based on two different bottom topographies: the first one

$$b(x)=5e^{-\frac{2}{5}(x-5)^2}\text{m}$$

is smooth, and the second one

$$b(x)=\begin{cases} 4\text{m}, & \text{if } 4\le x\le 8\text{m},\\ 0\text{m}, & \text{otherwise}, \end{cases}$$

is discontinuous. The initial conditions are at the still water still steady state

$$h+b=10\text{m} \quad \text{and} \quad u=0\text{m/s}$$

Table 1: L^1 and L^∞ errors over a smooth bottom topography.

Cells	Precision	L^1error		L^∞error	
		h	hu	h	hu
100	Single	$1.64E-07$	$1.65E-07$	$6.68E-07$	$4.84E-07$
	Double	$3.17E-14$	$2.63E-14$	$1.24E-14$	$9.55E-14$
200	Single	$1.03E-07$	$1.12E-07$	$5.32E-07$	$3.96E-07$
	Double	$2.55E-14$	$1.56E-14$	$1.09E-14$	$8.75E-14$

Table 2: L^1 and L^∞ errors over a discontinuous bottom topography.

Cells	Precision	L^1error		L^∞error	
		h	hu	h	hu
100	Single	$7.63E-07$	$1.29E-07$	$7.47E-07$	$7.95E-07$
	Double	$2.65E-14$	$2.45E-14$	$1.60E-14$	$9.07E-14$
200	Single	$5.19E-07$	$1.02E-07$	$5.69E-07$	$5.48E-07$
	Double	$1.35E-14$	$1.36E-14$	$1.03E-14$	$7.58E-14$

on the domain $[0,10]$m. To verify the well-balanced property numerically, we compute the errors between the solution at $t=0.5$s and the initial condition on meshes with 100 and 200 cells by single as well as double precisions respectively, then show them in Tables 1 and 2. The tables suggest that the errors are all at the level of machine accuracy and well-balanced WENO scheme is achieved correspondingly.

3.1.2 Testing the accuracy order

To test the fifth-order accuracy with smooth solutions, we choose the following initial data from [14]

$$h(x,0)=\left(5+e^{\cos(2\pi x)}\right)\text{m},\quad (hu)(x,0)=\sin(\cos(2\pi x))\text{m}^2/\text{s},$$

over a bottom topography $b(x)=\sin^2(\pi x)$m on $[0,1]$m. Periodic boundary conditions [14, 32] are imposed. Thanks to the non-existence of the exact solutions, we first apply the same scheme on a mesh with 12,800 cells to obtain reference solutions, and compute the L^1 errors as well as accuracy orders at $t=0.1$s, then present them in Table 3. The Table 3 implies that the expected fifth-order of accuracy orders are obviously achieved.

3.1.3 Perturbations of a steady state water flow

Herein, we utilize this example [38] to validate the capability to resolve small and large perturbations to a steady state. The bottom contains a bump

$$b(x)=\begin{cases} 0.25(\cos(10\pi(x-1.5))+1)\text{m}, & \text{if } 1.4\le x\le 1.6\text{m},\\ 0\text{m}, & \text{otherwise},\end{cases}$$

Table 3: L^1 errors and accuracy orders for the example in Section 3.1.2.

Cells	CFL	h		hu	
		L^1 error	Order	L^1 error	Order
25	0.6	$1.5947E-02$		$8.5321E-02$	
50	0.6	$2.5406E-03$	2.65	$1.7205E-02$	2.31
100	0.4	$2.9427E-04$	3.11	$2.2420E-03$	2.94
200	0.3	$2.2643E-05$	3.70	$1.8235E-04$	3.62
400	0.2	$9.4017E-07$	4.59	$7.4674E-06$	4.61
800	0.1	$2.9584E-08$	4.99	$2.3661E-07$	4.98

on $[0,2]$m. The initial data are given as follows

$$h(x,0)=\begin{cases}(1-b(x)+\epsilon)\text{m}, & \text{if } 1.1\le x\le 1.2\text{m},\\ (1-b(x))\text{m}, & \text{otherwise},\end{cases} \quad \text{and} \quad u(x,0)=0\text{m/s},$$

with $\epsilon>0$ being a perturbation parameter. We deal with $\epsilon=0.2$m (big pulse) and $\epsilon=0.001$m (small pulse) separately.

We present the free surface level $h+b$ and the flow discharge hu at $t=0.2$s against the reference solutions in Figs. 1 and 2. From the figures, we can obviously observe that both the pulses are all accurately resolved. Moreover, the solutions are free of spurious oscillations, and are comparable to those in the literature [14, 32, 38].

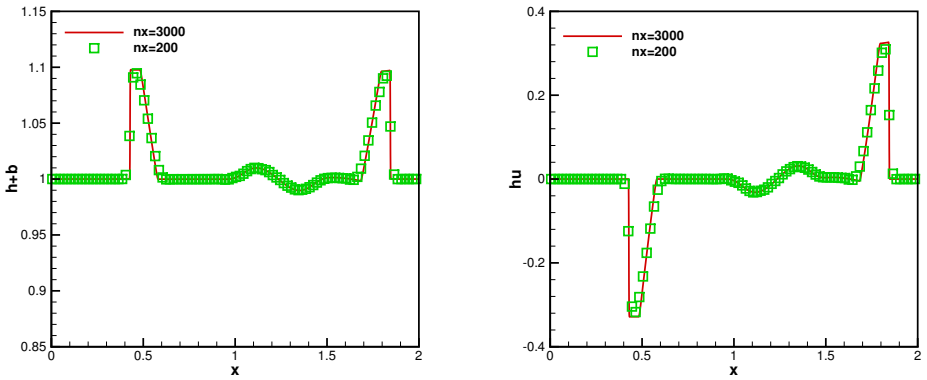

Figure 1: Perturbation of a steady state water flow with a big pulse. Free surface level $h+b$ (left) and flow discharge hu (right) at $t=0.2$s.

3.1.4 Steady flow over a hump

Then, we implement three benchmarks examples [39] to further validate the current schemes. The three examples contain transcritical, supercritical as well as subcritical

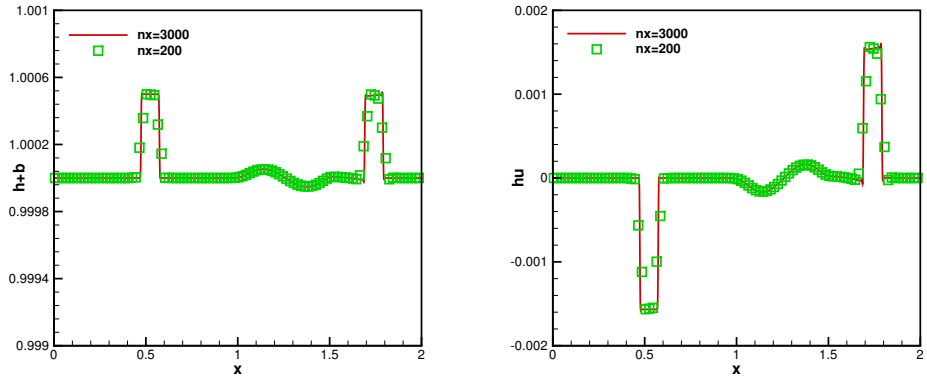

Figure 2: Perturbation of a steady state water flow with a small pulse. Free surface level $h+b$ (left) and flow discharge hu (right) at $t=0.2$s.

flows, respectively, over the following hump

$$b(x)=\begin{cases}(0.2-0.05(x-10)^2)\,\text{m}, & \text{if } 8\le x\le 12\text{m},\\ 0\text{m}, & \text{otherwise},\end{cases}$$

and are all coupled with the same initial data

$$h(x,0)=0.33\text{m} \quad \text{and} \quad u(x,0)=0\text{m/s},$$

on $[0,25]$m. Subsequently, we carry out all the computations on the same mesh with 200 cells up to $t=200$s and compare the numerical results with the exact solutions from [40].

- Case 1: Transcritical flow without a shock. We impose a unit discharge of $1.53\text{m}^2/\text{s}$ and an open boundary condition (i.e., $du/dx=0$) at the upstream boundary and on the downstream one, respectively. The $h+b$ and hu are shown in Fig. 3 and a very good agreement with the exact solutions is obviously achieved.

- Case 2: Transcritical flow with a shock. A water discharge of $0.18\text{m}^2/\text{s}$ and a water depth of 0.33m are imposed on the upstream boundary and on the downstream one, respectively. The free surface level $h+b$ and the water discharge hu against the exact solutions are shown in Fig. 4. The numerical results agree well with the exact ones and are free of spurious oscillations.

- Case 3: Subcritical flow. Similarly, we impose a water discharge of $4.42\text{m}^2/\text{s}$ and a water depth of 2m on the upstream boundary and on the downstream one, respectively. We demonstrate $h+b$ and hu in comparison with the exact solutions in Fig. 5. It is evident that the numerical results are in good agreement with the exact ones.

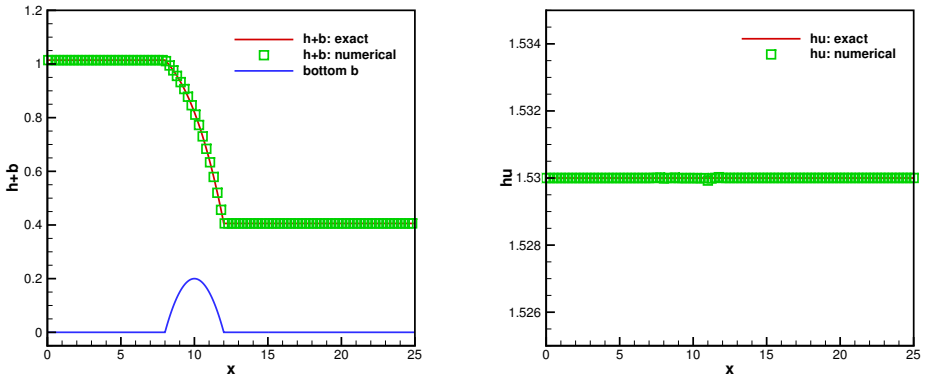

Figure 3: Transcritical flow without a shock. Free surface level $h+b$ (left) and flow discharge hu (right) at $t=200$s.

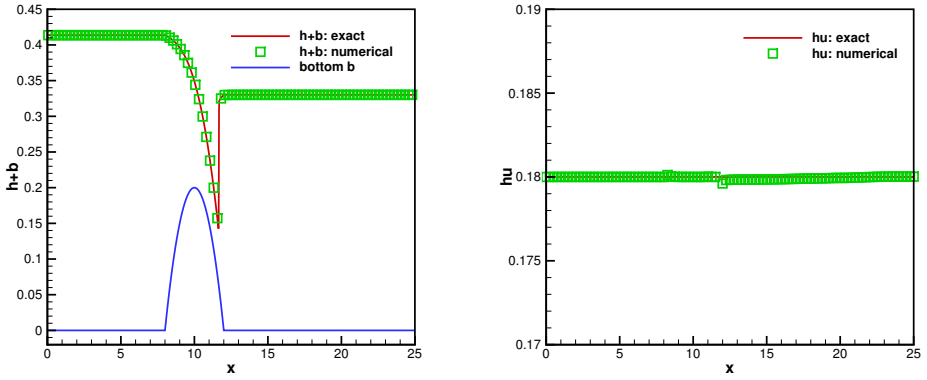

Figure 4: Transcritical flow with a shock. Free surface level $h+b$ (left) and flow discharge hu (right) at $t=200$s.

3.1.5 The dam break problem over a rectangular bump

Next, we implement a dam break test case from [12,14,32] on a rectangular shape bump:

$$b(x)=\begin{cases} 8\text{m}, & \text{if } \left|x-750\right|\leq 1500/8\text{m}, \\ 0\text{m}, & \text{otherwise}, \end{cases}$$

and consider the following initial data

$$h(x,0)=\begin{cases} (20-b(x))\text{m}, & \text{if } x\leq 750\text{m}, \\ (15-b(x))\text{m}, & \text{otherwise}, \end{cases} \qquad \text{and} \quad u(x,0)=0\text{m/s},$$

on $[0,1500]$m.

The numerical results are shown in Fig. 6, and keep a good agreement with the reference ones obviously.

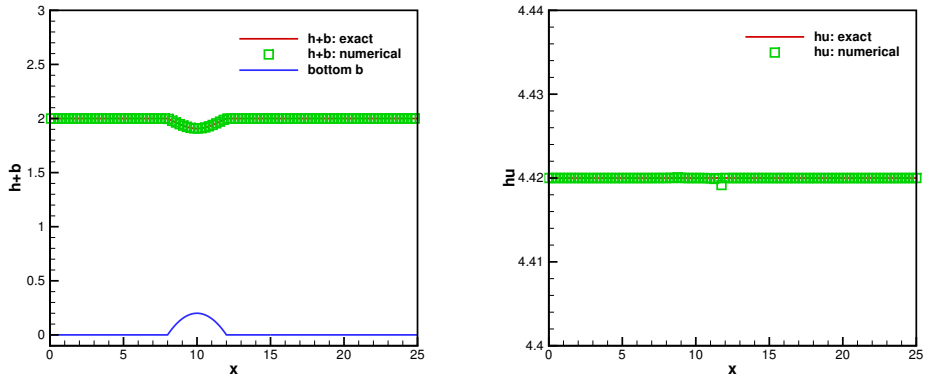

Figure 5: Subcritical flow. Free surface level $h+b$ (left) and flow discharge hu (right) at $t=200$s.

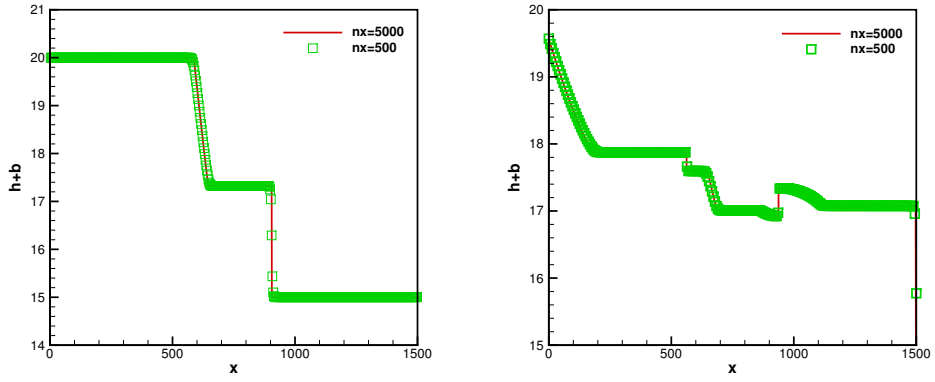

Figure 6: The dam break problem over a rectangular bump. Free surface level $h+b$ at $t=15$s (left) and $t=60$s (right).

3.1.6 The tidal wave flow

Then, we consider an example from [41] with the following initial data

$$h(x,0)=(60.5-b(x))\text{m}, \quad hu(x,0)=0\text{m}^2/\text{s},$$

over the following bottom topography

$$b(x)=\left(10+\frac{40x}{L}+10\sin\left(\pi\left(\frac{4x}{L}-\frac{1}{2}\right)\right)\right)\text{m},$$

with $L=14000$m as the length of the domain. The boundary condition

$$h(0,t)=\left(64.5-4\sin\left(\pi\left(\frac{4t}{86400}+\frac{1}{2}\right)\right)\right)\text{m}, \quad hu(L,t)=0\text{m}^2/\text{s},$$

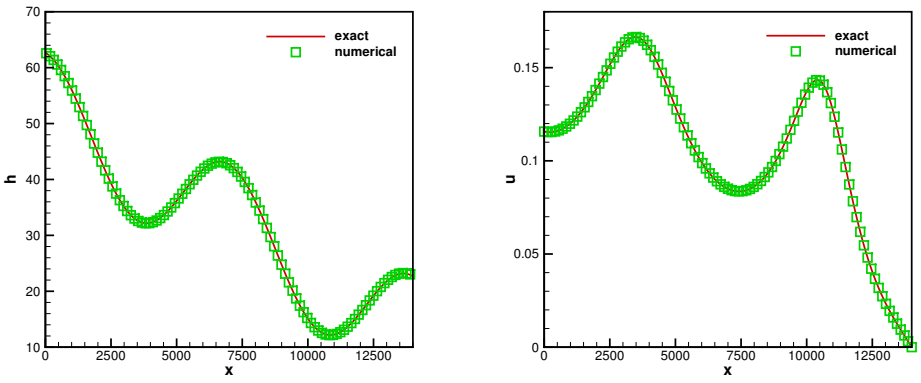

Figure 7: The tidal wave flow. Water depth h (left) and flow velocity u (right) at $t=7552.13$s.

is imposed at both ends of the computational domain. The exact solutions in the following form

$$h(x,t)=\left(64.5-b(x)-4\sin\left(\pi\left(\frac{4t}{86400}+\frac{1}{2}\right)\right)\right)\text{m},$$
$$hu(x,t)=\frac{(x-L)\pi}{5400}\cos\left(\pi\left(\frac{4t}{86400}+\frac{1}{2}\right)\right)\text{m}^2/\text{s},$$

can be obtained with the aid of the asymptotion analysis as in [41].

Numerical results at $t=7552.13$s against the exact solutions are shown in Fig. 7, and are obviously consistent with the exact ones.

3.1.7 The 1-rarefaction and 2-shock problem

To further testify our schemes, we consider an example over a step shape bottom [42]

$$b(x)=\begin{cases}0\text{m}, & \text{if } x\leq 0\text{m},\\ 1\text{m}, & \text{otherwise},\end{cases}$$

with the initial data

$$h(x,0)=\begin{cases}4\text{m}, & \text{if } x\leq 0\text{m},\\ 1\text{m}, & \text{otherwise},\end{cases}\qquad \text{and}\quad u(x,0)=0\text{m/s},$$

on $[-10,10]$m.

This example will produce a rarefaction moving to the left and a shock to the right over time. Numerical results at $t=1$s are shown in Fig. 8 and are evidently in good agreement with the exact ones.

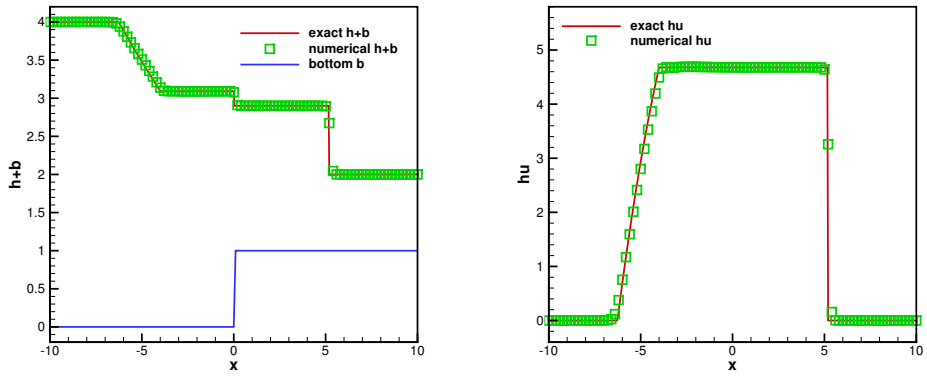

Figure 8: The 1-rarefaction and 2-shock problem. Free surface level $h+b$ (left) and flow discharge hu (right) at $t=1$s.

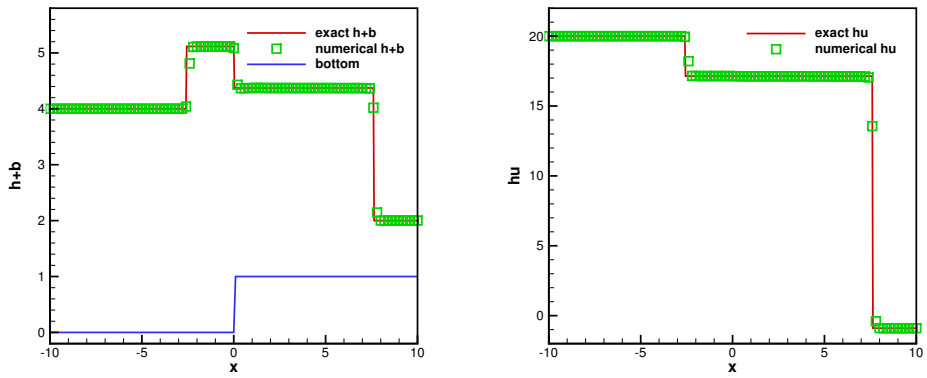

Figure 9: The 1-shock and 2-shock problem. Free surface level $h+b$ (left) and flow discharge hu (right) at $t=1$s.

3.1.8 The 1-shock and 2-shock problem

This example is also over the same step shape bottom as in Section 3.1.7 on $[-10,10]$m, and is accompanied by the following initial data

$$h(x,0)=\begin{cases} 4\text{m}, & \text{if } x\leq 0\text{m},\\ 1\text{m}, & \text{otherwise}, \end{cases} \qquad u(x,0)=\begin{cases} 5\text{m/s}, & \text{if } x\leq 0\text{m},\\ -0.9\text{m/s}, & \text{otherwise}. \end{cases}$$

As time goes on, this example will develop two shocks: one shock moving to the left and another one to the right. Numerical solutions at $t=1$s in comparison with the exact solutions are shown in Fig. 9 and agree well with the exact ones obviously.

3.2 Two-dimensional cases

3.2.1 Testing the well-balanced property

To testify the well-balanced property even for the two-dimensional case, we consider an example from [14] with the initial data

$$h(x,y,0)=(1-b(x,y))\text{m}, \quad u(x,y,0)=v(x,y,0)=0\text{m/s},$$

over the following bottom $b(x,y)=0.8e^{-50\left((x-0.5)^2+(y-0.5)^2\right)}\text{m}$ on the unity domain $[0,1]\text{m}\times[0,1]\text{m}$.

The L^1 errors between the solutions at $t=0.1$s and the initial data with different precisions are demonstrated in Table 4, and are all at the level of machine accuracy even for different precisions, then verify the expected well-balanced property correspondingly.

Table 4: L^1 errors for different precisions for the still water steady state solutions.

Cells	Precision	L^1error		
		h	hu	hv
100×100	Single	$2.51E-07$	$3.26E-06$	$5.41E-07$
	Double	$4.35E-15$	$2.18E-15$	$3.52E-15$
200×200	Single	$1.37E-07$	$2.29E-06$	$3.45E-07$
	Double	$2.95E-15$	$1.58E-15$	$2.57E-15$

3.2.2 Testing the accuracy order

By means of this example, we further check the orders of accuracy for the following two-dimensional problem. The initial data and the bottom topography are given by as in [14]

$$\begin{aligned}
&h(x,y,0)=10+e^{\sin(2\pi x)}\cos(2\pi y)\text{m},\\
&hu(x,y,0)=\sin(\cos(2\pi x))\sin(2\pi y)\text{m}^2/\text{s},\\
&hv(x,y,0)=\cos(2\pi x)\cos(\sin(2\pi x))\text{m}^2/\text{s},\\
&b(x,y,)=\sin(2\pi x)+\cos(2\pi y)\text{m},
\end{aligned}$$

on an unit square $[0,1]\text{m}\times[0,1]\text{m}$. We impose periodic boundary conditions and compute this example up to $t=0.05$s. Because the exact solution does not exist, we apply the same fifth-order scheme on a mesh with 1600×1600 cells to obtain a reference solution, and then take this reference solution as the exact solution to compute the numerical errors as well as the orders of accuracy. We present the errors and orders of accuracy in Table 5 and can observe that the fifth-order accuracy is achieved even for this two-dimensional example.

Table 5: L^1 errors and accuracy orders for the example in Section 3.2.2.

Cells	CFL	h		hu		hv	
		L^1 error	Order	L^1 error	Order	L^1 error	Order
25×25	0.6	$7.87E-03$		$3.25E-02$		$5.79E-02$	
50×50	0.6	$1.10E-03$	2.83	$4.44E-03$	2.87	$7.65E-03$	2.92
100×100	0.6	$1.74E-04$	3.67	$4.15E-04$	3.42	$5.84E-04$	3.71
200×200	0.4	$8.08E-06$	4.43	$2.54E-05$	4.03	$2.58E-05$	4.50
400×400	0.3	$2.80E-07$	4.85	$9.92E-07$	4.68	$9.08E-07$	4.83
800×800	0.2	$8.75E-09$	5.00	$3.12E-08$	4.99	$2.81E-08$	5.01

3.2.3 A small perturbation of a two-dimensional steady state water flow

In the end, we handle an example from [14,38] with the following initial data

$$h(x,y,0)=\begin{cases}(1-b(x,y)+0.01)\text{m}, & \text{if } 0.05\le x\le 0.15\text{m},\\ (1-b(x,y))\text{m}, & \text{otherwise},\end{cases}$$
$$u(x,y,0)=v(x,y,0)=0\text{m/s},$$

over an elliptical bump bottom

$$b(x,y)=0.8e^{-5(x-0.9)^2-50(y-0.5)^2}\text{m}$$

on a domain $[0,2]\text{m}\times[0,1]\text{m}$.

The contours of $h+b$ on two meshes at different final times are shown in Fig. 10 for comparison. The numerical results strongly imply that the current schemes enjoy the capability to resolve complex features of the water flow very well. Furthermore, the results here can also be compared with those in the literature [14,32].

4 Conclusions

This article develops well-balanced finite volume WENO schemes for one- and two-dimensional SWEs with geometrical source term. A suitable conservative variables decomposition strategy in combination with the hydrostatic reconstruction idea help us to construct well-balanced numerical fluxes. Moreover, this decomposition strategy also enables us to realize a novel and simple source term approximation, which is consistent with the approximation to the flux gradient. Rigorous theoretical analysis and extensive numerical evidences all verify the well-balanced property. Furthermore, numerical results indicate that the current schemes keep high-order accuracy for smooth solutions, and enjoy good resolutions for discontinuous solutions at the same time.

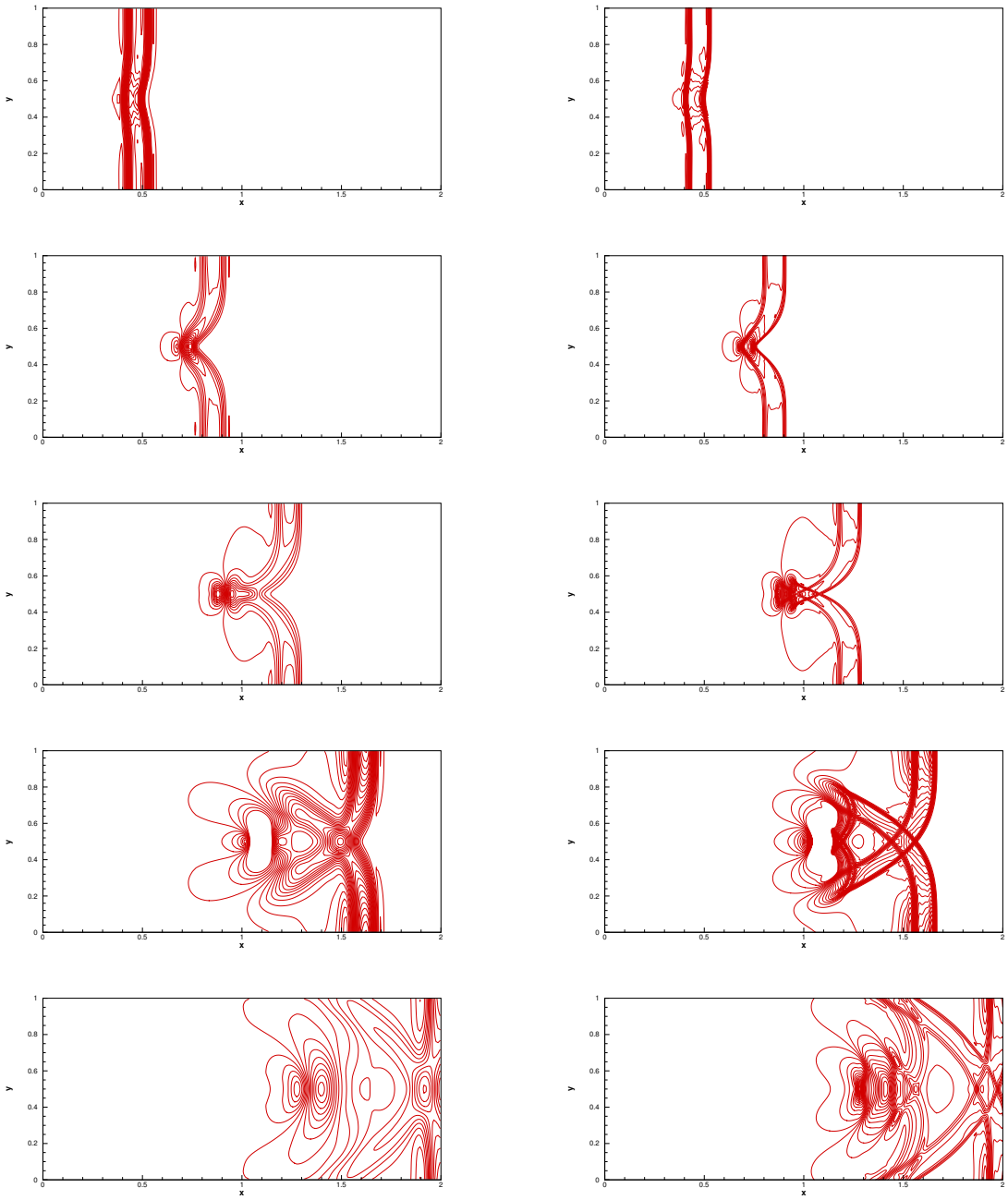

Figure 10: A small perturbation of a two-dimensional steady state water flow. Thirty equally spaced contours of $h+b$ at different final time. From top to bottom: at $t=0.12$s from 0.99942m to 1.00656m; at $t=0.24$s from 0.99318m to 1.01659m; at $t=0.36$s from 0.98814m to 1.01161m; at $t=0.48$s from 0.99023m to 1.00508m; and at $t=0.6$s from 0.99514m to 1.00629m. Left: 200×100 cells. Right: 600×300 cells.

Acknowledgements

This work is supported by the National Natural Science Foundation of China (No. 11771228).

References

[1] S. F. BRADFORD, AND B. F. SANDERS, *Finite volume model for shallow water flooding of arbitrary topography*, J. Hydraul. Eng., 128 (2002), pp. 289–298.
[2] G. GOTTARDI, AND M. VENUTELLI, *Central scheme for the two-dimensional dam-break flow simulation*, Adv. Water Resour., 27 (2004), pp. 259–268.
[3] C. B. VREUGDENHIL, Numerical Methods for Shallow-Water Flow, Springer, Dordrecht, pp. 15–25, 1995.
[4] J. M. GREENBERG, AND A. Y. LEROUX, *A well-balanced scheme for the numerical processing of source terms in hyperbolic equations*, SIAM J. Numer. Anal., 33 (1996), pp. 1–16.
[5] J. M. GREENBERG, A. Y. LEROUX, R. BARAILLE AND A. NOUSSAIR, *Analysis and approximation of conservation laws with source terms*, SIAM J. Numer. Anal., 34 (1997), pp. 1980–2007.
[6] S. NOELLE, Y. L. XING AND C.-W. SHU, High-Order Well-Balanced Schemes, Numerical Methods for Balance Laws, G. Puppo and G. Russo, editors, Quaderni di Mathematica, 2010.
[7] Y. L. XING, C.-W. SHU AND S. NOELLE, *On the advantage of well-balanced schemes for moving-water equilibria of the shallow water equations*, J. Sci. Comput. 48 (2011), pp. 339–349.
[8] B. PERTHAME, AND C. SIMEONI, *A kinetic scheme for the Saint-Venant system with a source term*, Calcolo, 38 (2001), pp. 201–231.
[9] K. XU, *A well-balanced gas-kinetic scheme for the shallow-water equations with source terms*, J. Comput. Phys., 178 (2002), pp. 533–562.
[10] A. KURGANOV, AND D. LEVY, *Central-upwind schemes for the Saint-Venant system,* Mathematical Modelling and Numerical Analysis, Esaim-Math. Model. Numer., 36 (2002), pp. 397–425.
[11] M. LUKÀČOVÀ-MEDVID'OVÀ, AND Z. VLK, *Well-balanced finite volume evolution Galerkin methods for the shallow water equations with source terms*, Int. J. Numer. Methods Fluids, 47 (2005), pp. 1165–1171.
[12] S. VUKOVIC, AND L. SOPTA, *ENO and WENO schemes with the exact conservation property for one-dimensional shallow water equations*, J. Comput. Phys., 179 (2002), pp. 593–621.
[13] S. VUKOVIC, N. CRNJARIC-ZIC AND L. SOPTA, *WENO schemes for balance laws with spatially varying flux*, J. Comput. Phys., 199 (2004), pp. 87–109.
[14] Y. L. XING, AND C.-W. SHU, *High order finite difference WENO schemes with the exact conservation property for the shallow water equations*, J. Comput. Phys., 208 (2005), pp. 206–227.
[15] S. NOELLE, N. PANKRATZ, G. PUPPO AND J. NATVIG, *Well-balanced finite volume schemes of arbitrary order of accuracy for shallow water flows*, J. Comput. Phys., 213 (2006), pp. 474–499.
[16] Y. L. XING, AND C.-W. SHU, *High order well-balanced finite volume WENO schemes and discontinuous Galerkin methods for a class of hyperbolic systems with source terms*, J. Comput. Phys., 214 (2006), pp. 567–598.
[17] G. LI, V. CALEFFI AND Z. K. QI, *A well-balanced finite difference WENO scheme for shallow water flow model*, Appl. Math. Comput., 265 (2015), pp. 1–16.
[18] Z. WANG, J. ZHU AND N. ZHAO, *A new robust high-order weighted essentially non-oscillatory scheme for solving well-balanced shallow water equations*, Adv. Appl. Math. Mech., 11 (2019), pp. 911–941.

[19] V. CALEFFI, *A new well-balanced Hermite weighted essentially non-oscillatory scheme for shallow water equations*, Int. J. Numer. Methods Fluids, 67 (2011), pp. 1135–1159.
[20] G. RUSSO, Central Schemes for Balance Laws, Proceedings of the VIII International Conference on Nonlinear Hyperbolic Problems, Magdeburg, 2000.
[21] R. TOUMA, AND S. KHANKAN, *Well-balanced unstaggered central schemes for one and two-dimensional shallow water equation systems*, Appl. Math. Comput., 218 (2012), pp. 5948–5960.
[22] A. ERN, S. PIPERNO AND K. DJADEL, *A well-balanced Runge-Kutta discontinuous Galerkin method for the shallow-water equations with flooding and drying*, Int. J. Numer. Methods Fluids, 58 (2008), pp. 1–25.
[23] G. VIGNOLI, V. A. TITAREV AND E. F. TORO, *ADER schemes for the shallow water equations in channel with irregular bottom elevation*, J. Comput. Phys., 227 (2008), pp. 2463–2480.
[24] A. NAVAS-MONTILLA, AND J. MURILLO, *Energy balanced numerical schemes with very high order, the augmented Roe flux ADER scheme, application to the shallow water equations*, J. Comput. Phys., 290 (2015), pp. 188–218.
[25] G. J. GASSNER, A. R. WINTERS AND D. A. KOPRIVA, *A well balanced and entropy conservative discontinuous Galerkin spectral element method for the shallow water equations*, Appl. Math. Comput., 272 (2016), pp. 291–308.
[26] Z. GAO, AND G. H. HU, *High order well-balanced weighted compact nonlinear schemes for shallow water equations*, Commun. Comput. Phys., 22 (2017), pp. 1049–1068.
[27] X. H. YUAN, *A well-balanced element-free Galerkin method for the nonlinear shallow water equations*, Appli. Math. Comput., 331 (2018), pp. 46–53.
[28] L. GOSSE, Computing Qualitatively Correct Approximations of Balance Laws, Springer, Milan, 2013.
[29] Y. XING, AND C.-W. SHU, *A survey of high order schemes for the shallow water equations*, J. Math. Study, 47 (2014), pp. 221–249.
[30] E. AUDUSSE, F. BOUCHUT, M. O. BRISTEAU, R. KLEIN AND B. PERTHAME, *A fast and stable well-balanced scheme with hydrostatic reconstruction for shallow water flows*, SIAM J. Sci. Comput., 25 (2004), pp. 2050–2065.
[31] E. AUDUSSE, AND M. O. BRISTEAU, *A well-balanced positivity preserving "second-order" scheme for shallow water flows on unstructured meshes*, J. Comput. Phys., 206 (2005), pp. 311–333.
[32] Y. L. XING, AND C.-W. SHU, *A new approach of high order well-balanced finite volume WENO schemes and discontinuous Galerkin methods for a class of hyperbolic systems with source terms*, Commun. Comput. Phys., 1 (2006), pp. 100–134.
[33] G. LI, L. N. SONG AND J. M. GAO, *High order well-balanced discontinuous Galerkin methods based on hydrostatic reconstruction for shallow water equations*, J. Comput. Appl. Math., 340 (2018), pp. 546–560.
[34] C.-W. SHU, Essentially non-oscillatory and weighted essentially non-oscillatory schemes for hyperbolic conservation laws, NASA/CR-97-206253, ICASE Report No. 97-65.
[35] C.-W. SHU, *High order weighted essentially nonoscillatory schemes for convection dominated problem*, SIAM Rev., 51 (2009), pp. 82–126.
[36] C.-W. SHU, *High order WENO and DG methods for time-dependent convection-dominated PDEs: Abrief survey of several recent developments*, J. Comput. Phys., 316 (2016), pp. 598–613.
[37] C.-W. SHU, AND S. OSHER, *Efficient implementation of essentially non-oscillatory shock-capturing schemes*, J. Comput. Phys., 77 (1998), pp. 439–471.
[38] R. J. LEVEQUE, *Balancing source terms and flux gradient on high-resolution Godunov methods: the quasi-steady wave-propagation algorithm*, J. Comput. Phys., 146 (1998), pp. 346–365.
[39] M. E. VAZQUEZ-CENDON, *Improved treatment of source terms in upwind schemes for the shallow*

water equations in channels with irregular geometry, J. Comput. Phys., 148 (1999), pp. 497–526.

[40] N. GOUTAL, AND F. MAUREL, Proceedings of the second workshop on dam-break wave simulation, Technical Report HE-43/97/016/A, Electricitè de France, Dèpartement Laboratoire National d'Hydraulique, Groupe Hydraulique Fluviale, 1997.

[41] A. BERMUDEZ, AND M. E. VAZQUEZ, *Upwind methods for hyperbolic conservation laws with source terms*, Comput. Fluids, 23 (1994), pp. 1049–1071.

[42] F. ALCRUDO, AND F. BENKHALDOUN, *Exact solutions to the Riemann problem of the shallow water equations with a bottom step*, Comput. Fluids, 30(6) (2001), pp. 643–671.